

# Visualizing Point Cloud Classifiers by Curvature Smoothing

Chen Ziwen  
Grinnell College  
Grinnell, IA

chenziwe@grinnell.edu

Wenxuan Wu  
Oregon State University  
Corvallis, OR

wuwen@oregonstate.edu

Zhongang Qi  
Oregon State University  
Corvallis, OR

qiz@oregonstate.edu

Li Fuxin  
Oregon State University  
Corvallis, OR

lif@oregonstate.edu

## Abstract

Recently, several networks that operate directly on point clouds have been proposed. There is significant utility in understanding them better, so that humans can understand more about the mechanisms how those networks classify point clouds, potentially helping diagnosing them and designing better architectures and data augmentation pipelines. In this paper, we propose a novel approach to visualize important features used in classification decisions of point cloud networks. Following ideas in visualizing 2-D convolutional networks, our approach is based on gradually smoothing parts of the point cloud. However, different from the 2-D case, we smooth the curvature of the point cloud to remove sharp shape features. The resulting point cloud is then evaluated on the original point cloud network to see whether the performance has dropped or remained the same, from which parts that are important to the point cloud classification are identified. A technical contribution of the paper is an approximated curvature smoothing algorithm, which can smoothly transition from the original point cloud to one of constant curvature, such as a uniform sphere. With this smoothing algorithm, we propose PCI-GOS, a 3-D extension of the Integrated-Gradients Optimized Saliency (I-GOS) algorithm, as a perturbation-based visualization technique realized on 3-D shapes. Experiment results revealed insights into these classifiers.

## 1. Introduction

Recently, direct deep learning on unstructured 3-D point clouds has gained significant interest. Many interesting point cloud networks have been proposed. PointNet++ [20] utilizes max-pooling followed by multi-layer perceptron. PointConv [30] realizes a convolution operation on point

clouds efficiently. DGCNN [29] builds on PointNet++ by learning features from edges instead of vertices. SPLAT-Net [25] embeds features into a high-dimensional lattice and applies convolution on the lattice. Other works such as [32, 3, 14, 8, 27] all have their own merits. As with 2-D image classifiers, we are curious about what these models have actually learned. Following [9]’s definition of *explanations* as meta-predictors, we want to *explain* those models by identifying which parts of a shape contribute most to the final score, and which parts the least. Such an explanation would help us gain more insights, diagnose the networks, and potentially design better network structures and data augmentation pipelines.

A natural representation of this *explanation* is a heatmap, which associates each point (pixel) with an importance score. To show that a heatmap is valid, following the *deletion* and *insertion* metric proposed by [19], we should expect the predicted score to drop quickly when we “cover up” important features, indicated by heated parts in the heatmap, and to rise quickly when we gradually “reveal” *only* the most important features.

Here we put “cover up” and “reveal” in quotes because they have not been defined yet on 3-D data. It is easy to “cover up” some parts of a 2-D image: simply turn those pixels into grey or black, or apply a significant Gaussian blur to those pixels. It is not easy to extend this notion to 3-D point clouds, since however we move the points, they will always be part of the point cloud, and thus contributing to the underlying shape. We can directly delete points as in prior work [34], but many current point-based deep networks are not robust to direct deletion, and not all networks even accept inputs with varying number of points.

Our goal is to perform this “cover up” process in a manner so that the resulting point cloud has the same number of points as before, and does not create irregular shapes that

fall outside the training distribution. Hence, we attempt to smoothly morph the 3-D shape to remove distinctive shape features, such as edges and corners. With the key observation that edges and corners are reflected by abnormal curvatures on the underlying surface, we specify the goal of our smoothing algorithm to be averaging the curvature on the underlying surface of the point cloud (thus the final shape should have approximately constant curvature everywhere).

In this paper, we propose a novel smoothing algorithm to achieve this goal. For each point in the point cloud, a local plane is fit to its neighborhood. We prove under some conditions that the distance from the point to this local plane is a valid approximation of the local mean curvature (see Appendix A). This allows us to utilize a diffusion-based smoothing algorithm, which can gradually average out the approximated curvature on the underlying surface. For instance, if the underlying surface is closed, then our algorithm will gradually morph the shape into a sphere.

With the new smoothing method, we propose PCI-GOS (“point-cloud I-GOS”), a 3-D extension of a recent 2-D heatmap visualization algorithm [21]. We experiment our approach on PointConv [30] and DGCNN [29], two state-of-the-art point cloud networks. Results on the ModelNet40 dataset reveals that, different from image-based networks that often classify based on a small distinctive feature, point-based networks usually rely heavily on the entire shape to classify. Still, certain important parts can be found so that once distorted, the score will drop quickly. Besides, symmetry is very important for the networks to recognize certain classes. We believe that these results improve our understanding of those networks and may help improving their design in the future.

## 2. Related Work

**Classifier visualization** Using heatmaps to visualize networks has attracted much research effort these years. There are two main categories of approaches: gradient-based and perturbation-based. Gradient-based approaches utilizes the gradients of the output score w.r.t. the input as the standard of measuring input contribution [23, 33, 24, 4, 22, 26]. Perturbation-based methods, on the other hand, perturb the input and examine which parts of the input have the largest influence on the output. Object detectors in CNNs [35], Real Time Image Saliency [6], Meaningful Perturbation [9], RISE [19] and I-GOS [21] belong to this family.

As far as we know none of these methods have been tried on 3-D point cloud classifiers. [34] is the only prior work we know that attempts to visualize point cloud networks. [34] uses a gradient-based approach and calculates the gradients of the output score with respect to the straight line from median to the input points and regards those gradients as saliency. However, their method only works well for networks that have a max-pooling layer, and otherwise requires

retraining of the classifier to take into account the irregular shape they created, whereas our goal is to be applicable to any type of deep network model without re-training.

A close relative of perturbation-based visualization is adversarial attack [31, 16], in that both tasks seek the smallest change to the input that drop the prediction score of a deep network significantly. The difference between those methods are that visualization tasks want the perturbed features to be natural, so that if the perturbed features are the only that are present, the network can identify them and utilize them to correctly classify the shape. This is a property that usually does not hold for adversarial attacks. The recent perturbation method I-GOS[21] explicitly involved techniques to prevent a visualization perturbation from becoming adversarial.

**3-D shape morphology** There has been active research in smoothing and fairing 3-D structures. For mesh smoothing, [28] has proposed a method based on diffusion, and proved it to serve as a low-pass filter and is anti-shrinkage. However, as [7] pointed out, this diffusion method is flawed due to its unrealistic assumption about meshes. [7] proposed a scheme based on curvature flow, where a local “curvature normal” is computed at each vertex and the diffusion is based on it. Meshes are easier to smooth than point clouds because they provide readily estimated planes that can be used to compute curvature. Some noise-removal scheme that directly operates on point clouds were proposed in [1] and [18]. Most of these methods are based on moving least-squares [13] with a local plane/surface fitting. However, the goals of these approaches are mainly removing noises, rather than gradually morphing the shape to one with constant curvature as in our goal.

In terms of mathematical morphology, several work aimed to extend well-known 2-D morphological operations to point clouds [5, 15]. In [5], a point set surface is fitted for the point cloud to get a signed distance function (SDF) representation for the point cloud, and then a point structuring element (PSE), which is a SDF itself, is fitted for each point using mean shift. Finally, the morphological projection of the point can be computed using the PSE. [15] proposed a purely point-based approach for defining the Minkowski sum for point clouds, which is fast and simple. In their approach, a structuring element (SE) is a set of vectors, which are all added to each point in the in order to perform one iteration. Then a decimation step removes the points inside the boundary. However, most of these techniques require the shape to be closed and orientable, i.e., have an “inside” and an “outside”, both being assumptions we would not like to make in order to render our algorithm more generally applicable.

### 3. Methods

Throughout this paper we work on a point cloud with  $N$  points, denoted as  $\mathbf{P} = [p_1, \dots, p_N]$ , where  $p_i \in \mathbb{R}^3$  is a 3-tuple of  $x, y, z$  coordinates. Denote a neighborhood of  $p_i$  as  $\mathcal{N}(p_i)$  and  $K$  as the size of the neighborhood. Let  $\text{diag}(\cdot)$  represent the operator taking a vector and making it a diagonal matrix,  $\mathbf{I}$  be the identity matrix, and  $\mathbf{1}$  to be the vector of all 1s.

#### 3.1. Smoothing Point Clouds

Our goal is to smoothly morph a point cloud into a feature-less shape. We regard ‘‘curvature’’ on the surface as features here, since edges and corners are all large curvatures on the surface that are distinct from their surroundings. Hence, we want the curvature on the entire point cloud to be constant or has little variance. Assuming the underlying manifold is closed, this goal is equivalent to morphing the shape into a sphere. If the shape is already on a plane, then we aim to make the curvature on its boundary constant, i.e., smoothing it into a disk. The total number of points should stay the same, and each point should be traceable from its initial position to its final position. In the following we first describe the classical Taubin smoothing [28] on meshes, then our algorithm.

##### 3.1.1 Taubin Smoothing

The local Laplacian at a vertex  $p_i$  is linearly approximated using the umbrella operator:

$$L(p_i) = \frac{1}{K} \sum_{j \in \mathcal{N}(p_i)} (p_j - p_i). \quad (1)$$

This approximation assumes unit-length edges and equal angles between two adjacent edges around a vertex [7].  $L(p_i)$  has a matrix form

$$L(\mathbf{P}) = -\mathbf{L}\mathbf{P} \quad (2)$$

where  $\mathbf{L} = \mathbf{D} - \mathbf{A}$  is the Laplacian matrix, assuming  $\mathbf{A}$  is the  $K$ -nearest neighbor graph adjacency matrix in  $\mathbf{P}$  and  $\mathbf{D} = \text{diag}(\mathbf{A}\mathbf{1})$  is the diagonal degree matrix of each point. Each vertex is then updated using the following scheme,

$$p'_i = p_i + \lambda L(p_i) \quad (3)$$

$$p''_i = p'_i - \mu L(p'_i) \quad (4)$$

where  $0 < \lambda < 1$  and  $\lambda < \mu$ . The main idea is that Eq.(3) refers to a diffusion operator equivalent to  $\mathbf{P} = (\mathbf{I} - \lambda\mathbf{L})\mathbf{P}$ , so that once this operation is carried out multiple times, most of the eigenvalues of  $\mathbf{L}$  become close to zero and henceforth the points become more evenly distributed. Note that if only Eq.(3) is carried out, then the point cloud will

ultimately collapse to a single mean. Hence, [28] proposed to add a step Eq.(4) to prevent shrinkage, so that the volume enclosed by the underlying manifold does not decrease. An intuition is that Eq. (3) attenuates the high frequencies and Eq. (4) magnifies the remaining low frequencies, thus preventing shrinkage. However, as [7] pointed out, this diffusion method is flawed due to its unrealistic assumption about meshes.



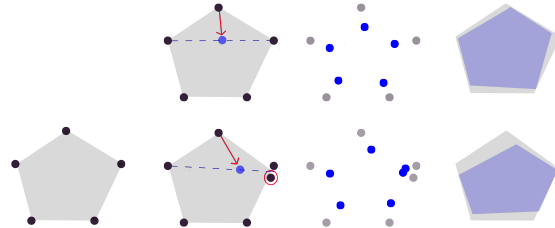
(a) Applying 3-D version of our algorithm to a car shape.



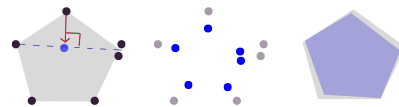
(b) Applying 2-D version of our algorithm to a curtain shape.

Figure 1: Demonstrations of our smoothing algorithm on two shapes from ModelNet40.

##### 3.1.2 Our algorithm



(a) Laplacian smoothing. The resulting shape is distorted by the addition of one single noisy point (the second row).



(b) Curvature normal smoothing based on plane fitting. If we use a locally fitted plane to update the position of the points, then the resulting shape does not distort due to uneven distribution of the points.

Figure 2: Comparison between (a) Laplacian smoothing and (b) the proposed curvature normal smoothing based on plane fitting. Left: original shape; Middle: smoothing results on the points; Right: Comparison between the underlying shapes of the original and new point set.

Based on the above diffusion formulation and with suit-

able parameter choices, Taubin smoothing should be able to smooth using any self-adjoint compact operator beyond the Laplacian operator [36]. [7] as an example smooths on the curvature normal operator. However, their curvature approximation requires the data in the form of a mesh, which is different from a point cloud. In this paper, we approximate the mean curvature at a point by calculating its distance to a plane locally fitted to its neighborhood. Fitting such a plane allows us to be more robust to noisy input point clouds (Fig. 2). Afterwards, utilizing Taubin’s algorithm, we gradually filter out high frequency changes in curvature on the underlying surface of the point cloud. If the underlying shape is a closed manifold, our algorithm will be able to smooth it into approximately a sphere, where curvature is constant everywhere. Additionally, our algorithm leaves the density distribution of the point cloud unchanged as shown in sec. 4.1, i.e., the distances between points remain roughly the same before and after morphing.

To fit a local plane  $H = \{x : \langle x, \mathbf{n} \rangle + D = 0, x \in \mathbb{R}^3\}$ ,  $\mathbf{n} \in \mathbb{R}^3, \|\mathbf{n}\| = 1$  for each point  $p_i$ , we minimize the least-squares error:

$$\arg \min_{\mathbf{n}, D} \sum_{j \in \mathcal{N}(p_i)} (\langle p_j, \mathbf{n} \rangle + D)^2 \quad (5)$$

Let  $h_i$  denote the position of  $p_i$  after being projected onto  $H$  (i.e.  $h_i = p_i - (\langle p_i, \mathbf{n} \rangle + D) \cdot \mathbf{n}$ ). Then  $h_i - p_i$  is the vector pointing from the point  $p_i$  to the plane  $H$ . Note that the direction of  $h_i$  is just the surface normal at  $p_i$ . However, we hold that the distance to the plane is an approximation to the mean curvature, and coincides with the curvature under some simplifying assumptions – see the Appdex A for a proof.

With that result, we can accommodate [28]’s smoothing algorithm to point cloud data as follows:

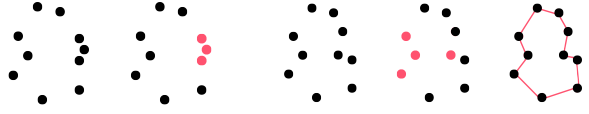
$$p'_i = p_i + \lambda (h_i - p_i) \quad (6)$$

$$p''_i = p'_i - \mu (h'_i - p'_i) \quad (7)$$

where  $0 < \lambda < 1$ ,  $\lambda < \mu$  and  $h'_i$  refers to the projection of  $p'_i$  on a new plane  $H'$  fitted for  $p'_i$ . Thus instead of moving the point toward the mean of its neighbors, we move it directly toward the locally fitted plane. We call Eq. 6 the “erosion” round, and Eq. 7 the “dilation” round.

An important implementation detail is that the size of the neighborhood we use increases as the smoothing goes further. In practice, after every 4 rounds of erosion and dilation, we expand the neighborhood size by 20 points. The reason for this is twofold. On one hand, there might exist isolated neighborhoods in a point cloud (i.e. a set of points that is closed under the  $\mathcal{N}(\cdot)$  operation) as shown in Fig. 3a. If the curvature information cannot be propagated to the entire point cloud, the algorithm will fail. On the other hand, a larger neighborhood speeds up the smoothing process. As

mentioned in [12], the time step restriction ( $0 < \lambda < 1$ ) results in the need of hundreds of updates to cause a noticeable smoothing using the original implementation in [28]. Note that however, we also cannot make the neighborhood size too large, especially at the beginning, due to the “false neighbor” issue innate to the point cloud data structure (explained in Fig. 3b).



(a) The “isolated neighborhood” ( $K = 2$ ). The rightmost red dot is a false neighbor for the red dot in the center as the true underlying shape is indicated by the line drawing on the right.

Figure 3: Two issues innate to point clouds (due to the missing edge information between vertices).

To deal with degenerate cases where the point cloud is already on a plane, we further extend the algorithm to a 2-D case (Fig. 1b). Here the goal is to filter out high frequency changes in curvature on the boundary, transforming the plane to a disk. In this case, assuming all the neighborhood points  $\mathcal{N}(p_i)$  are on the plane, we fit a line  $H' = \{x : \langle x, \mathbf{n}' \rangle + C = 0, x \in \mathbb{R}^2\}$ ,  $\mathbf{n}' \in \mathbb{R}^2, \|\mathbf{n}'\| = 1$  for  $w_i = (0, 0)$  by minimizing the least-squares error:

$$\arg \min_{\mathbf{n}', C} \sum_{j \in \mathcal{N}(p_i)} (\langle p_j, \mathbf{n}' \rangle + C)^2 \quad (8)$$

where each  $w_j$  is the projection of  $p_j$  to the plane  $(\vec{u}, \vec{v})$ . Let  $q_i$  be  $p_i$ ’s projection on line  $H'$ . We update  $p_i$  in the same fashion as in the 3-D case:

$$w'_i = w_i + \lambda (q_i - w_i) \quad (9)$$

$$w''_i = w'_i - \mu (q'_i - w'_i) \quad (10)$$

Denote the final 2D coordinates as  $w_T = (u_T, v_T)$ , we convert it back to 3-D by calculating  $p'_i = p_i + u_T \vec{u} + v_T \vec{v}$ . In reality, due to noises, many points are not exactly on a plane. We project them to their local planes  $H$  first, and then calculate the  $uv$ -coordinates from their projected location  $h_i$ . Note that we still shift the point from its original location  $p_i$ , not its projected location  $h_i$ . In actual implementation, the 2-D version is used together with the 3-D version and is always run first. For example, in an “erosion” round, we run Eq. (9) first, then Eq. (6); in a “dilation” round, we run Eq. (10) first, then Eq. (7). Empirically this seems to generalize well on both planar and non-planar surfaces, we believe the reason is that on non-planar surfaces the line fitting usually falls close to the point itself, hence the planar version hardly



moves any point at all. By utilizing both of them at every iteration, we avoid introducing an extra threshold to decide whether a neighborhood is on a plane.

### 3.2. Visualizing Point Cloud Classifiers

We first summarize I-GOS [21], a recent algorithm for visualizing deep networks. The goal in I-GOS is to optimize for a small and smooth mask so that when an image is masked, the prediction from the deep network drops significantly. I-GOS improves from the conventional gradient descent approaches in that the optimization is solved with descent steps based on *integrated gradients*. The reason not to use conventional gradients alone is that the integrated gradients may more likely point to a global optimum for the unconstrained problem of only minimizing the prediction on the image, so that the optimization can evade local optima and achieve better performance. I-GOS has obtained state-of-the-art performance on multiple image resolutions, better than earlier popular algorithms in that it can find a small mask that pinpoints to important parts of the image.

We seek to adapt this algorithm to point clouds. Formally, let mask  $\mathbf{M}$  be of the same size as the point cloud  $\mathbf{P}$ , and initialized with all zeros. Let  $\mathbf{P}_0$  be the fully smoothed point cloud (e.g. sphere) and let  $\mathbf{M}_0 = \mathbf{1}\mathbf{1}^\top$  be the baseline mask, so that when applied to the shape, the shape becomes  $\mathbf{P}_0$ . Mask values are always between  $[0, 1]$ , where 0 means no smoothing and 1 means fully smoothing. We optimize the mask by minimizing the classification score on the masked point cloud, along with two regularizers:

$$\min_{\mathbf{M}} \widehat{L}_{cls}(f_c(\cdot), \mathbf{P}, \mathbf{M}) + \lambda_{l1} L_{l1}(\mathbf{M}) + \lambda_{tv} L_{tv}(\mathbf{M}) \quad (11)$$

where

$$\widehat{L}_{cls} = \frac{1}{S} \sum_{s=1}^S f(\Phi(\mathbf{P}, \mathbf{M} + \frac{s}{S}(\mathbf{M}_0 - \mathbf{M}))) \quad (12)$$

where  $S$  is the number of intervals used ( $S = 20$  in our experiment). The gradient of this loss function is exactly the integrated gradients used in [26].  $\widehat{L}_{cls}$  is an approximation to the *integrated* classification score loss along the straight path from  $\mathbf{M}_0$  to  $\mathbf{M}$ :

$$L_{cls} = \int_{\alpha=0}^1 f_c(\Phi(\mathbf{P}, \mathbf{M} + \alpha(\mathbf{M}_0 - \mathbf{M}))) d\alpha \quad (13)$$

where  $f_c(\cdot)$  represents the classifier on the class  $c$  to be visualized (usually the class with the highest predicted confidence) and  $\Phi$  represents the action of applying the mask to the point cloud.

Besides, we have  $L_{l1} = \frac{1}{N} \|\mathbf{1} - \mathbf{M}\|_1$  and  $L_{tv} = \frac{1}{N} \sum_{\mathbf{M}} \frac{1}{K} \sum_{j \in \mathcal{N}(p_i)} |m_j - m_i|$ , the total variation regularization. The  $L_1$  and TV regularizations are to make the

mask small and smooth, hence making the resulting point cloud more likely to stay in the same distribution as the training set and less likely to be adversarial.

One difficulty in extending this algorithm to 3-D point clouds is to implement  $\Phi(\cdot)$  as a differentiable masking operation. In 2-D images, we can simply use a weighted (by  $m_i$ ) average of the actual pixel value and the baseline pixel value. However, in point clouds, if we directly push a point toward its corresponding baseline position, undesirable (out-of-distribution) sharp structure might appear.

Ideally, we want to smooth more on the points with higher mask value, and less on the points with lower mask value. Unfortunately, this process leads to an undifferentiable  $\Phi(\cdot)$ . In practice, we make  $\Phi(\cdot)$  differentiable by pre-computing 10 intermediate shapes with increasing level of smoothness. We approximate the ideal mask smoothing operation by combining the 10 shapes:

$$\Phi(p_i, m_i) = \frac{\sum_{l=0}^{10} \exp(-\alpha \|10 \cdot m_i - l\|^2) p_{i,l}}{\sum_{l=0}^{10} \exp(-\alpha \|10 \cdot m_i - l\|^2)} \quad (14)$$

where  $p_i$  is a point with a mask value  $m_i \in [0, 1]$ ,  $l$  refers to the  $l$ -th point cloud in our sequence of precomputed smoothed shapes ( $l = 10$  refers to  $\mathbf{P}_0$  and  $l = 0$  refers to the original shape), and  $p_{i,l}$  refers to the position of the  $i$ -th point in the  $l$ -th point cloud.

We optimize Eq. (11) for the mask  $\mathbf{M}$ . Our new algorithm PCI-GOS shares several important traits with its 2-D counterpart: 1) the masks converge quickly (we typically only need 30 steps of optimization for each shape), and 2) the resulting masks make small changes to the original point clouds with a large impact on the prediction score, and are interpretable by human (as shown in Fig. 7).

## 4. Experiments

We have conducted two types of experiments. First, we compare our new smoothing algorithm against a number of baselines to validate its smoothing capability. Second, we utilize PCI-GOS to visualize point cloud classifiers and compare with some baselines as well as performing some ablation studies on the visualization. All experiments are conducted on the test split of the ModelNet40 dataset, with the classifiers trained on the training split. Each shape contains 1024 randomly sampled points, and only  $xyz$  location information is used in all experiments. All parameters of our smoothing algorithm are fixed for all shapes:  $\lambda = 0.7$ ,  $\mu = 1.0$ ,  $K$  grows from 20 to 60. We usually run the algorithm for 80 iterations on each shape (each iteration contains one ‘‘erosion’’ step and one ‘‘dilation’’ step).

### 4.1. Point cloud smoothing

Since there were few prior works that directly smooth point clouds, we compare against several other plausible

Table 1: Comparison of point cloud smoothing algorithms. Mesh refers to meshing and smoothing. Taubin refers to directly applying Taubin smoothing to point clouds. As shown in this table, only our algorithm succeeds in both morphing the shape into a feature-less sphere and keeping the morphing process smooth. For  $l = 0$  (initial shapes), CSD=0.10, MR=0.83.

Algorithm	Metric										
Smoothing level		1	2	3	4	5	6	7	8	9	10
Mesh	CSD	0.10	0.10	0.11	0.12	0.13	0.14	0.16	0.17	0.19	0.20
	MR	0.82	0.82	0.82	0.82	0.82	0.83	0.86	0.85	0.83	0.83
	DDS	0.40	0.67	0.62	0.63	0.60	0.58	0.48	0.38	0.40	0.30
Taubin	CSD	0.10	0.11	0.11	0.11	0.11	0.11	0.10	0.10	0.09	0.09
	MR	0.83	0.84	0.83	0.87	0.88	0.86	0.86	0.86	0.75	0.73
	DDS	0.90	0.92	0.74	0.87	0.83	0.81	0.69	0.74	0.43	0.66
Quadratic	CSD	0.11	0.12	0.12	0.12	0.12	0.12	0.13	0.13	0.13	0.13
	MR	0.79	0.80	0.81	0.81	0.83	0.83	0.83	0.84	0.83	0.83
	DDS	0.76	0.83	0.84	0.89	0.82	0.89	0.92	0.92	0.88	0.94
Ours	CSD	0.08	0.07	0.07	0.06	0.06	0.06	0.06	0.06	0.06	<b>0.05</b>
	MR	0.85	0.87	0.88	0.89	0.91	0.92	0.94	0.94	0.95	<b>0.95</b>
	DDS	0.60	0.75	0.68	0.72	0.64	0.66	0.59	0.60	0.56	0.58

baselines. First note that directly applying Gaussian blur to point coordinates is not a valid baseline, because Gaussian blur tends to smooth the coordinate values, which results in pushing neighboring points to all have the same coordinates, leading to a skeleton effect which is completely contrary to our goals. We mainly compare against three baselines:

**Meshing, then smoothing.** One natural idea is to convert the point cloud to a mesh and then apply mesh-based smoothing techniques such as [7] to the result. For our goals, we need to choose an algorithm that does not change the number of points and maintain a 1-1 correspondence with the original point cloud. We utilized a greedy projection triangulation algorithm [17], but due to the noisiness and sparsity of the point cloud, the meshing result is often not ideal, as well as the smoothing results (e.g. Fig. 5).

**Directly applying mesh smoothing techniques to points.** Instead of explicit meshing, we can use neighborhood function  $\mathcal{N}(\cdot)$  to construct an *implicit mesh*, i.e., assuming a point has an edge to each of the points in its neighborhood. Using this implicit mesh, mesh smoothing techniques can be applied directly to point clouds. However, the uneven distribution of points in a point cloud quite often distorts the result, in a method such as Taubin smoothing (Fig. 4). Though [10] and [7] have proposed improvements for irregular meshes, they explicitly exploit edge information, which is not available in point cloud data (and requires explicit meshing as above).

**Fitting a quadratic surface.** Another natural idea is to directly fit a quadratic surface to the local neighborhood instead of a plane as in our approach. A quadratic surface allows analytic computation of the curvature which is in principle a better approximation than the plane. We implemented the closed-form quadratic fitting algorithm follow-

ing [11]. However, as pointed out by [2], since quadratic surfaces have a large degree of freedom compared to planes (10 parameters compared to 4), even a small bit of noise will render an undesired quadratic type or direction. As illustrated in Fig. 6, the border of the car shape ends up consisting of quadratic lines curving outward instead of inward.

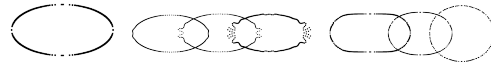


Figure 4: Left: A 2-D ellipse shape with 202 unevenly distributed points. Middle: Taubin smoothing. Right: Our smoothing. In the case of Taubin smoothing, highly concentrated areas are pushing points outward, resulting in an undesired shape (i.e., more frequent change in curvature), while our algorithm is not influenced by point density (and thus, the constant curvature is achieved as desired).

For a quantitative comparison against these baselines, we propose **three** metrics to evaluate our smoothing algorithm: *curvature standard deviation* (CSD), *min-max ratio* (MR) and *density distribution similarity* (DDS). The first two are to ensure the final shape is feature-less as desired, and the last one is to ensure the morphing process does not bring abrupt changes to the point cloud. In practice, ten intermediate point clouds with increasing level of blurriness are sampled. The metrics are calculated for all of them and the averaged results across the entire ModelNet40 testing set are listed in Table 1.

**CSD.** We regard large curvature on a shape as “features”, and we want to eliminate those “features” through the smoothing algorithms. As we remove the most distinct curvatures on the surface like edges and corners, the standard deviation of the curvatures will decrease, due to the elimination of the large outliers. In our experiment, we measure the distance from each point to its locally fitted

Table 2: Insertion and Deletion results on PointConv and DGCNN averaged over 40 classes, as well as ablation study for  $l1$ -loss and  $tv$ -loss using *deletion* and *insertion* metrics. As shown, both losses are necessary for maximizing the performance of the algorithm.

	PointConv			DGCNN		
	<i>deletion</i>	<i>insertion</i>	difference	<i>deletion</i>	<i>insertion</i>	difference
no $l1$ , no $tv$	0.2833	0.3889	0.1056	0.1825	0.2212	0.0387
with $l1$ , no $tv$	0.2710	0.3989	0.1279	0.1659	0.2264	0.0605
no $l1$ , with $tv$	<b>0.2677</b>	0.4097	0.1420	<b>0.1563</b>	0.2234	0.0670
with $l1$ , with $tv$	0.2684	<b>0.4113</b>	<b>0.1429</b>	0.1594	<b>0.2315</b>	<b>0.0720</b>

Table 3: Mean classification score for the 40 classes over 100 randomly sampled fully blurred spherical shapes (PointConv). It can be seen that a blurred spherical shape is mostly classified to the flowerpot, plant or vase classes. Hence the results of the current approach would only be applicable on the rest 37 classes.

airplane	bathhtub	bed	bench	bookshelf	bottle	bowl	car	chair	cone
0.0022	0.0002	0.0012	0.0031	0.0005	0.0036	0.0000	0.0010	0.0114	0.0130
cup	curtain	desk	door	dresser	flowerpot	glassbox	guitar	keyboard	lamp
0.0024	0.0139	0.0128	0.0002	0.0000	0.2242	0.0001	0.0134	0.0000	0.0204
laptop	mantel	monitor	nightstand	person	piano	plant	radio	rangehood	sink
0.0000	0.0000	0.0002	0.0000	0.0025	0.0021	0.3699	0.0262	0.0000	0.0045
sofa	stairs	stool	table	tent	toilet	tv stand	vase	wardrobe	xbox
0.0009	0.0322	0.0003	0.0005	0.0222	0.0004	0.0002	0.2121	0.0000	0.0004

Table 4: Baseline methods for obtaining saliency mask compared to PCI-GOS using the *deletion* and *insertion* metrics (averaged over 40 classes), conducted with the PointConv classifier.

	<i>deletion</i>	<i>insertion</i>	difference
mask-only	<b>0.2318</b>	0.2474	0.0156
ig-only	0.3751	0.3099	-0.0653
PCI-GOS	0.2684	<b>0.4113</b>	<b>0.1429</b>

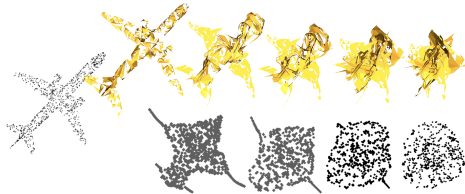


Figure 5: Upper row: meshing a point cloud and then applying Laplacian smoothing. Lower row: our smoothing algorithm.



Figure 6: Upper row: mean-curvature-flow algorithm utilizing curvature from fitted quadratic surfaces to local neighborhoods. Lower row: our smoothing algorithm.

plane ( $K = 60$ ) as an approximation of the local mean curvature. While we realize this approximation is not perfect, we use the results in Table 1 to show that our smoothing

algorithm is indeed working.

**MR.** Assuming that the underlying manifold is closed, our smoothing should eventually morph the point cloud into a sphere. Hence, we propose to evaluate the ratio between the length on the short side and the long side of the point cloud. This is computed by first applying principal component analysis (PCA) to the point cloud and finding the top two principal components, say  $\vec{u}$  and  $\vec{v}$ . Then we compute the ratio between ranges of the values on these two principal directions. The closer this ratio is to 1, the better. As shown in Table 1, our algorithm achieves the highest final MR.

**DDS.** We want the morphing process to be smooth in that the density distribution of each point cloud to *remain the same* throughout the morphing process. We conduct the kernel density estimation at each point (using a Gaussian kernel with  $\sigma = 0.1$ ) to obtain the density distribution of the entire point cloud, and then compare the similarity between the distributions of two consecutive blurred levels using the Kolmogorov-Smirnov test (p-values are recorded as results). As shown in Table 1, all methods are able to keep the distributions reasonably close.

From the experiment results, all baseline algorithms fail to eliminate large curvatures on the surface. Their curvature variance has even increased for some blurred levels. All of them fail to improve MR at all, which means the final shape is not sphere-like as desired. Only our algorithm succeeds in both removing features from the surface and keeping the morphing process smooth.

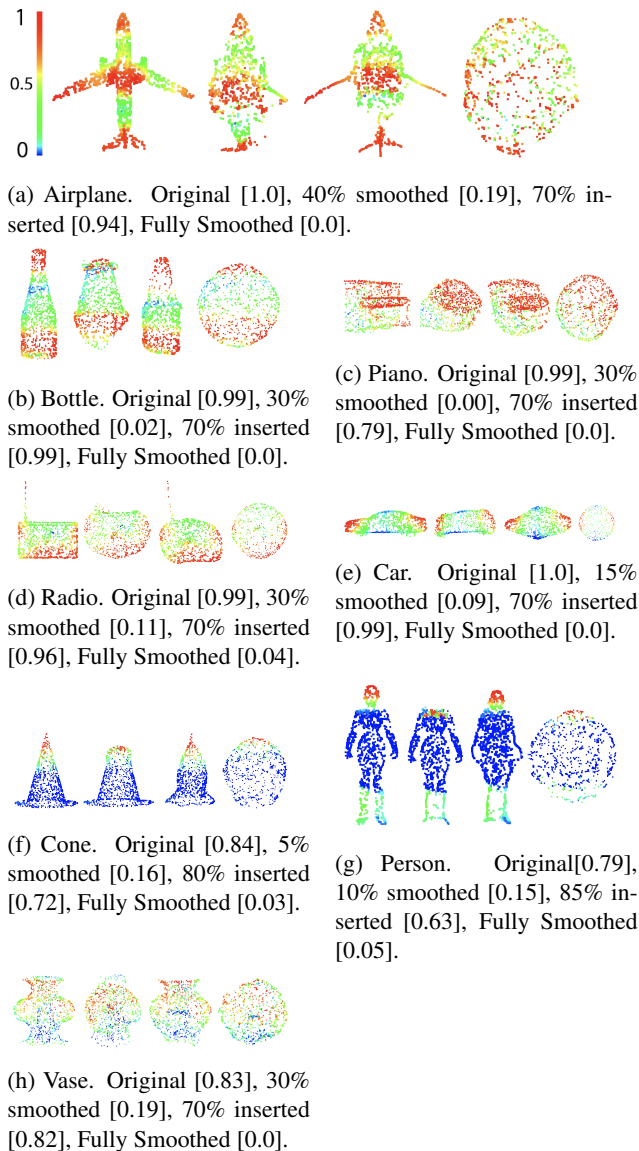


Figure 7: Example masks (best viewed in color). First four for PointConv, last four for DGCNN. Red indicates highly important points, blue for least important ones (maximal importance is 1 as indicated in the colorbar at the top-left corner). Within each group of pictures from left to right: original shape, least percentage of points smoothed to drop the prediction confidence below  $0.2 \times$  original confidence, least percentage of points inserted for rising the prediction above  $0.8 \times$  original prediction confidence, 100% blurred. Numbers within square brackets are the prediction confidence for the corresponding shape.

## 4.2. Classifier visualization

We experiment our new PCI-GOS algorithm on PointConv [30] and DGCNN [29], two state-of-the-art point cloud classifiers. Both networks have classification accuracy above 92% on the ModelNet 40 test set. Fig. 7 shows some example masks generated by our algorithm for Point-

Conv and DGCNN. These pictures reveal to us some interesting insight into the patterns used in the classifiers: for airplanes, the wings and the tails are crucial; for radios, the existence of the antenna is critical; for cars, the front and the trunk are important; for vases, the curvature at the neck is more important than the curvature at the bottom. Compared with 2D images, 3D point clouds generally needs a much higher percentage of points to be inserted for the classifier to make a sensible prediction, which indicates that they often require the global shape information to classify while many 2D categories can be discriminated by local texture features [21]. How to reconcile this difference in a dataset with both point cloud and RGB could lead to interesting future network designs.

We use the *deletion* and *insertion* metrics proposed by [19] to evaluate the heatmaps. For *deletion*, we gradually smooth the shape from the largest points to the smallest ones. Then we obtain the curve of network prediction confidences on the differently smoothed shapes and the metric is the area under the curve. The *insertion* metric is also the area under a prediction confidence curve, but the curve is created by gradually inserting important points in the cloud without smoothing, only leaving the most unimportant points to be smoothed. We want the *deletion* score to be low, indicating that smoothing a small area would distract the classifier, and the *insertion* score to be high, indicating that the classifier can predict from a small amount of features. Experiment results averaged over all 40 classes are shown in the last row of Table 2. The supplementary materials show some of the curves from each category.

Table 4 shows the comparison between the two baseline methods and PCI-GOS: mask-only [9] and ig-only [26]. Mask-only learns the mask using gradients instead of integrated gradients. Each mask goes through 300 iterations under this method, as opposed to 30 under PCI-GOS. Ig-only directly takes a one-step integrated gradient instead of an optimization process. From the table we can see that PCI-GOS performs much better than the baselines. Table 2 shows the ablation study for  $l1$ -loss and  $tv$ -loss ( $tv$  stands for total-variation). As we can see, both losses are useful for maximizing the performance of the algorithm.

One issue that is unique to point cloud smoothing is that, the fully-smoothed spherical shaped cloud may still have semantic meaning, different from 2D images where there is usually no information in a completely blurred image. In Table. 3 we took 100 random completely smoothed point clouds (spherical) and classified them with PointConv. The result showed significant confidence on 3 classes: vase, flowerpot and plant. This indicates that maybe the current visualizations will not be informative in these 3 classes. Alternative approaches to define “featureless” or non-informative point clouds are interesting future work.



## 5. Conclusions and Future Work

In this paper, we propose PCI-GOS, a classifier visualization approach by extending the I-GOS algorithm to point cloud classifiers. In order to smooth the point clouds without abrupt changes, we proposed a novel approximated curvature normal smoothing approach. Experiment results show that our algorithm outperforms baselines on both point cloud smoothing and classifier visualization.

Our experiment results for visualization shows that the 3-D shapes consistently give higher deletion metric score and lower insertion metric score compared to the 2-D results in [21], indicating that point cloud networks usually need a more holistic shape to be classified compared with 2-D image CNNs. Besides, the spherical shape at the end of smoothing could still be classified as some semantic classes, again different from 2D. We hope the visualization results in this paper improve the understanding on those new point cloud networks and we look forward to exploring better definitions of “non-informative” point clouds as well as smoothing with features beyond curvature in future work.

## References

- [1] Marc Alexa, Johannes Behr, Daniel Cohen-Or, Shachar Fleishman, David Levin, and Claudio T Silva. Point set surfaces. In *Proceedings of the Conference on Visualization '01*, pages 21–28. IEEE Computer Society, 2001. 2
- [2] James Andrews and Carlo H Séquin. Type-constrained direct fitting of quadric surfaces. *Computer-Aided Design and Applications*, 11(1):107–119, 2014. 6
- [3] Matan Atzmon, Haggai Maron, and Yaron Lipman. Point convolutional neural networks by extension operators. *arXiv preprint arXiv:1803.10091*, 2018. 1
- [4] Sebastian Bach, Alexander Binder, Grégoire Montavon, Frederick Klauschen, Klaus-Robert Müller, and Wojciech Samek. On pixel-wise explanations for non-linear classifier decisions by layer-wise relevance propagation. *PLoS one*, 10(7):e0130140, 2015. 2
- [5] Stéphane Calderon and Tamy Boubekeur. Point morphology. *ACM Trans. Graph.*, 33(4):45:1–45:13, July 2014. 2
- [6] Piotr Dabkowski and Yarín Gal. Real time image saliency for black box classifiers. In *Advances in Neural Information Processing Systems*, pages 6967–6976, 2017. 2
- [7] Mathieu Desbrun, Mark Meyer, Peter Schröder, and Alan H Barr. Implicit fairing of irregular meshes using diffusion and curvature flow. In *Proceedings of the 26th annual conference on Computer graphics and interactive techniques*, pages 317–324. Citeseer, 1999. 2, 3, 4, 6, 11
- [8] Matthias Fey, Jan Eric Lenssen, Frank Weichert, and Heinrich Müller. Splinecnn: Fast geometric deep learning with continuous b-spline kernels. In *Proceedings of the IEEE Conference on Computer Vision and Pattern Recognition*, pages 869–877, 2018. 1
- [9] Ruth C. Fong and Andrea Vedaldi. Interpretable explanations of black boxes by meaningful perturbation. In *The IEEE International Conference on Computer Vision (ICCV)*, Oct 2017. 1, 2, 8
- [10] Koji Fujiwara. Eigenvalues of laplacians on a closed riemannian manifold and its nets. *Proceedings of the American Mathematical Society*, 123(8):2585–2594, 1995. 6
- [11] Bennett Groshong, Griff Bilbro, and Wesley Snyder. Fitting a quadratic surface to three dimensional data. 1989. 6
- [12] Leif Kobbelt, Swen Campagna, Jens Vorsatz, and Hans-Peter Seidel. Interactive multi-resolution modeling on arbitrary meshes. In *Siggraph*, volume 98, pages 105–114, 1998. 4
- [13] David Levin. The approximation power of moving least-squares. *Mathematics of computation*, 67(224):1517–1531, 1998. 2
- [14] Yangyan Li, Rui Bu, Mingchao Sun, Wei Wu, Xinhan Di, and Baoquan Chen. Pointcnn: Convolution on x-transformed points. In *Advances in Neural Information Processing Systems*, pages 820–830, 2018. 1
- [15] Jyh-Ming Lien. Point-based minkowski sum boundary. In *15th Pacific Conference on Computer Graphics and Applications (PG'07)*, pages 261–270. IEEE, 2007. 2
- [16] Daniel Liu, Ronald Yu, and Hao Su. Extending adversarial attacks and defenses to deep 3d point cloud classifiers. *arXiv preprint arXiv:1901.03006*, 2019. 2
- [17] Zoltan Csaba Marton, Radu Bogdan Rusu, and Michael Beetz. On Fast Surface Reconstruction Methods for Large and Noisy Datasets. In *Proceedings of the IEEE International Conference on Robotics and Automation (ICRA)*, Kobe, Japan, May 12-17 2009. 6
- [18] Boris Mederos, Luiz Velho, and Luiz Henrique de Figueiredo. Robust smoothing of noisy point clouds. In *Proc. SIAM Conference on Geometric Design and Computing*, volume 2004, page 2, 2003. 2
- [19] Vitali Petsiuk, Abir Das, and Kate Saenko. Rise: Randomized input sampling for explanation of black-box models. *arXiv preprint arXiv:1806.07421*, 2018. 1, 2, 8
- [20] Charles R. Qi, Li Yi, Hao Su, and Leonidas J. Guibas. Pointnet++: Deep hierarchical feature learning on point sets in a metric space. In *Advances in Neural Information Processing Systems 30*, pages 5099–5108. Curran Associates, Inc., 2017. 1
- [21] Zhongang Qi, Saeed Khorrani, and Fuxin Li. Visualizing deep networks by optimizing with integrated gradients. In *AAAI Conference on Artificial Intelligence*, 2020. 2, 5, 8, 9
- [22] Avanti Shrikumar, Peyton Greenside, Anna Shcherbina, and Anshul Kundaje. Not just a black box: Learning important features through propagating activation differences. *arXiv preprint arXiv:1605.01713*, 2016. 2
- [23] Karen Simonyan, Andrea Vedaldi, and Andrew Zisserman. Deep inside convolutional networks: Visualising image classification models and saliency maps. *arXiv preprint arXiv:1312.6034*, 2013. 2
- [24] Jost Tobias Springenberg, Alexey Dosovitskiy, Thomas Brox, and Martin Riedmiller. Striving for simplicity: The all convolutional net. *arXiv preprint arXiv:1412.6806*, 2014. 2
- [25] Hang Su, Varun Jampani, Deqing Sun, Subhansu Maji, Evangelos Kalogerakis, Ming-Hsuan Yang, and Jan Kautz.



- Splatnet: Sparse lattice networks for point cloud processing. In *Proceedings of the IEEE Conference on Computer Vision and Pattern Recognition*, pages 2530–2539, 2018. 1
- [26] Mukund Sundararajan, Ankur Taly, and Qiqi Yan. Axiomatic attribution for deep networks. In *Proceedings of the 34th International Conference on Machine Learning - Volume 70, ICML'17*, pages 3319–3328. JMLR.org, 2017. 2, 5, 8
- [27] Maxim Tatarchenko, Jaesik Park, Vladlen Koltun, and Qian-Yi Zhou. Tangent convolutions for dense prediction in 3d. In *Proceedings of the IEEE Conference on Computer Vision and Pattern Recognition*, pages 3887–3896, 2018. 1
- [28] Gabriel Taubin. A signal processing approach to fair surface design. In *Proceedings of the 22Nd Annual Conference on Computer Graphics and Interactive Techniques, SIGGRAPH '95*, pages 351–358, New York, NY, USA, 1995. ACM. 2, 3, 4
- [29] Yue Wang, Yongbin Sun, Ziwei Liu, Sanjay E Sarma, Michael M Bronstein, and Justin M Solomon. Dynamic graph cnn for learning on point clouds. *arXiv preprint arXiv:1801.07829*, 2018. 1, 2, 8
- [30] Wenxuan Wu, Zhongang Qi, and Li Fuxin. Pointconv: Deep convolutional networks on 3d point clouds. In *The IEEE Conference on Computer Vision and Pattern Recognition (CVPR)*, June 2019. 1, 2, 8
- [31] Chong Xiang, Charles R Qi, and Bo Li. Generating 3d adversarial point clouds. In *Proceedings of the IEEE Conference on Computer Vision and Pattern Recognition*, pages 9136–9144, 2019. 2
- [32] Yifan Xu, Tianqi Fan, Mingye Xu, Long Zeng, and Yu Qiao. Spidercnn: Deep learning on point sets with parameterized convolutional filters. In *Proceedings of the European Conference on Computer Vision (ECCV)*, pages 87–102, 2018. 1
- [33] Matthew D Zeiler and Rob Fergus. Visualizing and understanding convolutional networks. In *European conference on computer vision*, pages 818–833. Springer, 2014. 2
- [34] Tianhang Zheng, Changyou Chen, Junsong Yuan, Bo Li, and Kui Ren. Pointcloud saliency maps. In *The IEEE International Conference on Computer Vision (ICCV)*, October 2019. 1, 2
- [35] Bolei Zhou, Aditya Khosla, Agata Lapedriza, Aude Oliva, and Antonio Torralba. Object detectors emerge in deep scene cnns. *arXiv preprint arXiv:1412.6856*, 2014. 2
- [36] Kehe Zhu. *Operator theory in function spaces*. Number 138. American Mathematical Soc., 2007. 4

# Appendices

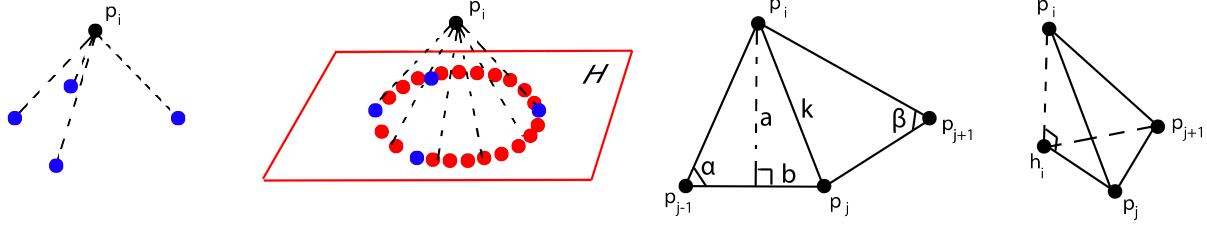


Figure 8: Auxillary graph for proof in Appendix A. From left to right: point  $p_i$  and its actual neighbors (in blue),  $p_i$  and its virtual neighbors (in red) and the fitted local plane  $H$ , enlarged graph of  $p_i$  and three of its neighbors,  $p_i$  and its projection  $h_i$  on the fitted plane  $H$ . Note that  $h_i$  is also the center of the ring formed by the virtual neighbors.

## A. Curvature approximation proof

Our proof will refer to Fig. 8.

We prove under some conditions that the distance from a point to its fitted local plane is a valid approximation of the local mean curvature. [7] has already showed that on a 3-D mesh, given a point  $p_i$  and its neighbors, the local “curvature normal” can be calculated using

$$\frac{1}{4A} \sum_{j \in \mathcal{N}(p_i)} (\cot \alpha_j + \cot \beta_j)(p_j - p_i) \quad (15)$$

where  $A$  is the sum of the areas of the triangles having  $p_i$  as common vertex and  $\alpha_j, \beta_j$  are the two angles opposite to the edge  $e_{ij}$  (i.e.  $p_j - p_i$ ). This arrangement is demonstrated Fig. 8.

Since point cloud data are usually sparse and noisy, we want to utilize some mechanism to mitigate this sparsity and irregularity. Here, we first fit a local plane to  $p_i$ 's neighborhood, and then we define the notion of “virtual neighbors” as a means to fill in the gaps left by the “actual neighbors”. We assume the “virtual neighbors” distribute evenly and densely on a ring surrounding  $p_i$  on the fitted plane  $H$ , each having the same distance  $k$  to  $p_i$  ( $k$  is calculated using the average distance of the actual neighbors). Let  $p_i$ 's projection on  $H$  be  $h_i$ , which is at the center of the ring formed by the “virtual neighbors”. Let  $a$  be the distance from  $p_i$  to each edge  $e_{j,j+1}$ . Let  $b$  be half of the length of  $e_{j,j+1}$ . Thus we can calculate  $A$  in Eq. 15 as  $n \cdot ab$ . Since we assumed the points are distributed evenly, we have  $\cot \alpha = \cot \beta = \frac{b}{a}$ . Thus we have the curvature normal

$$\text{to be } \frac{1}{4A} \sum_j (\cot \alpha_j + \cot \beta_j)(p_j - p_i) = \frac{1}{4nab} \cdot \frac{2b}{a} \sum_j (p_j - p_i) = \frac{1}{2na^2} \sum_j (p_j - p_i).$$

Note that the vector  $p_j - p_i$  is equal to  $(p_i - h_i) + (h_i - p_i)$ , and it can be easily shown that  $\sum_j (p_i - h_i) = \vec{0}$ . Thus we can continue derive the curvature normal to be  $\frac{1}{2na^2} \sum_j (p_j - p_i) = \frac{1}{2na^2} \sum_j (h_i - p_i) = \frac{n}{2na^2} (h_i - p_i) = \frac{1}{2a^2} (h_i - p_i)$ . Since we assume the points are distributed densely, thus we have as  $n \rightarrow \infty, a \rightarrow k$ . Hence, the curvature normal at  $p_i$  can be approximated by the expression

$$\frac{1}{2k^2} (h_i - p_i) \quad (16)$$

where  $h_i - p_i$  is just the vector pointing from  $p_i$  to the local plane  $H$  as in Eq. 6 and 7. This equation makes sense in that when the distance from  $p_i$  to  $H$  is fixed, the further away the neighbors are, the “flatter” the surface at  $p_i$  is.

In our actual experimentation however, we found that due to the extremely irregular distribution of the point cloud data, the neighborhood distance is misleading sometimes rather than helpful. Thus, in our final algorithm, we abandon the distance information  $\frac{1}{2k^2}$  and directly use the vector pointing from  $p_i$  to plane  $H$  as our approximation for the local curvature.

## B. Deletion and insertion scores

Table 5: *Deletion* score curve average and *insertion* score curve average for PointConv.

	airplane	bathtub	bed	bench	bookshelf	bottle	bowl	car	chair	cone
<i>del.</i>	0.5834	0.1859	0.1886	0.2557	0.3345	0.3084	0.2029	0.2917	0.4551	0.3720
<i>ins.</i>	0.6802	0.3052	0.3195	0.3343	0.4224	0.4907	0.3307	0.6385	0.6452	0.4672
	cup	curtain	desk	door	dresser	flowerpot	glassbox	guitar	keyboard	lamp
<i>del.</i>	0.1178	0.2386	0.1748	0.2112	0.1151	0.3486	0.0839	0.2331	0.2482	0.4263
<i>ins.</i>	0.3425	0.2315	0.2779	0.3261	0.2846	0.4730	0.1934	0.4470	0.3048	0.6227
	laptop	mantel	monitor	nightstand	person	piano	plant	radio	rangehood	sink
<i>del.</i>	0.2182	0.2283	0.2620	0.1429	0.1871	0.2872	0.7666	0.2601	0.2474	0.3175
<i>ins.</i>	0.3055	0.3728	0.4304	0.3545	0.2867	0.3822	0.8337	0.4626	0.3406	0.4408
	sofa	stairs	stool	table	tent	toilet	tv stand	vase	wardrobe	xbox
<i>del.</i>	0.2742	0.2521	0.1727	0.4009	0.3107	0.1933	0.1602	0.4210	0.0628	0.1446
<i>ins.</i>	0.3611	0.3779	0.3350	0.4656	0.7125	0.4644	0.2864	0.6709	0.1046	0.1644

Table 6: *Deletion* score curve average and *insertion* score curve average for DGCNN.

	airplane	bathtub	bed	bench	bookshelf	bottle	bowl	car	chair	cone
<i>del.</i>	0.3683	0.0683	0.1456	0.1473	0.2328	0.1501	0.1439	0.2661	0.3206	0.1905
<i>ins.</i>	0.4906	0.1158	0.1900	0.1980	0.2849	0.2972	0.1933	0.3740	0.4141	0.3338
	cup	curtain	desk	door	dresser	flowerpot	glassbox	guitar	keyboard	lamp
<i>del.</i>	0.0630	0.0714	0.1285	0.0674	0.0702	0.1082	0.0628	0.2503	0.1685	0.2269
<i>ins.</i>	0.0767	0.1511	0.1788	0.1413	0.0880	0.0983	0.0812	0.3875	0.2011	0.3464
	laptop	mantel	monitor	nightstand	person	piano	plant	radio	rangehood	sink
<i>del.</i>	0.0534	0.0782	0.2127	0.0860	0.1091	0.1554	0.6798	0.2013	0.1018	0.1196
<i>ins.</i>	0.0675	0.1077	0.2972	0.1262	0.4150	0.2031	0.7188	0.2466	0.1560	0.2267
	sofa	stairs	stool	table	tent	toilet	tv stand	vase	wardrobe	xbox
<i>del.</i>	0.1840	0.1677	0.1366	0.1761	0.1918	0.1362	0.0924	0.1706	0.0463	0.0584
<i>ins.</i>	0.2306	0.2285	0.1920	0.1932	0.2626	0.2498	0.1086	0.3781	0.0654	0.0745

## C. Curve figures

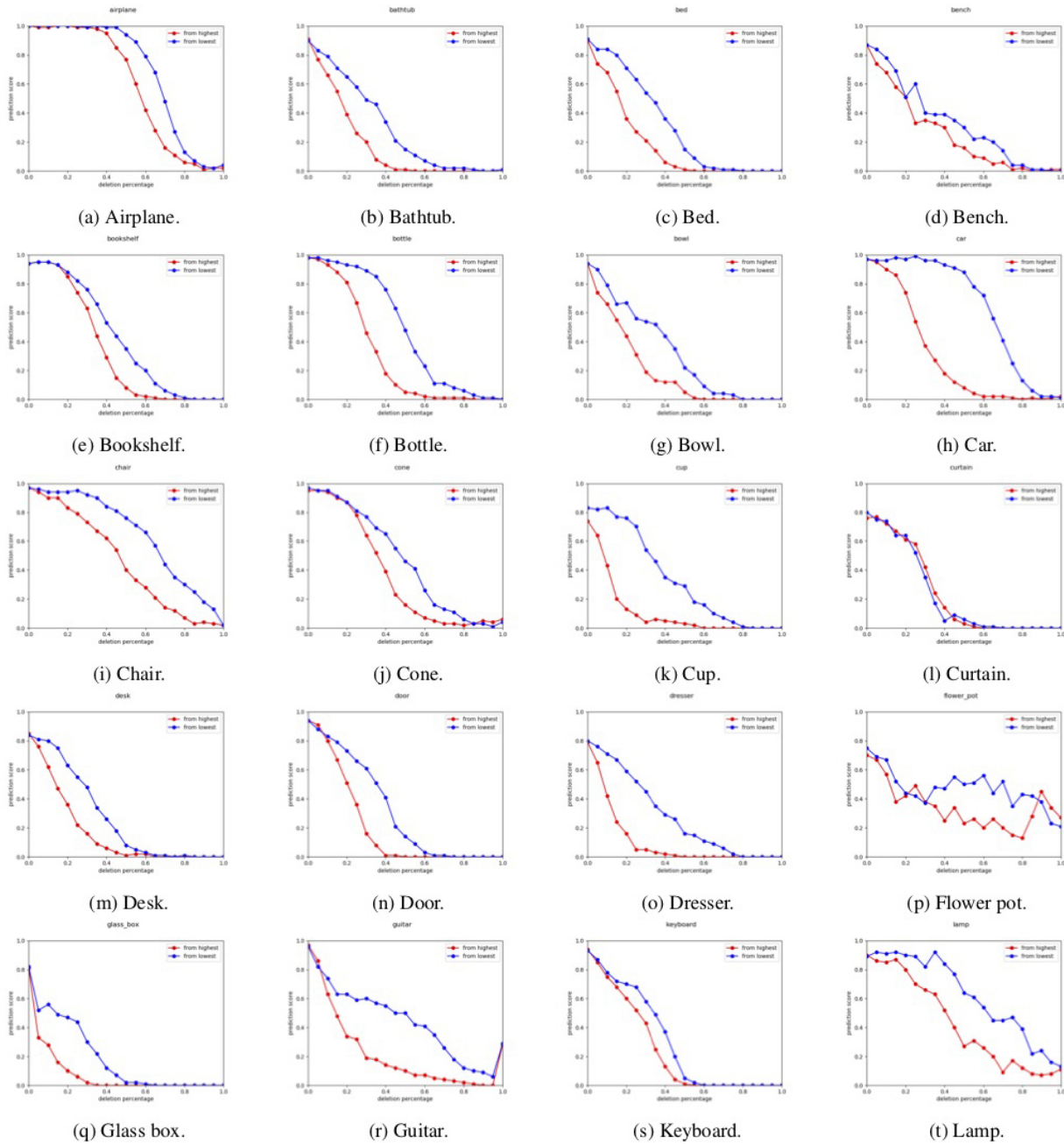


Figure 9: *Deletion* and *insertion* curves for all 40 classes in ModelNet40 for PointConv. Horizontal axis is the deletion percentage (top 5%, 10%, etc.), and vertical axis is the predicted class score. The red line is the *deletion* curve which blurs points from highest mask values, and the blue line is the *insertion* curve (if read from right to left) which blurs points from lowest mask values.

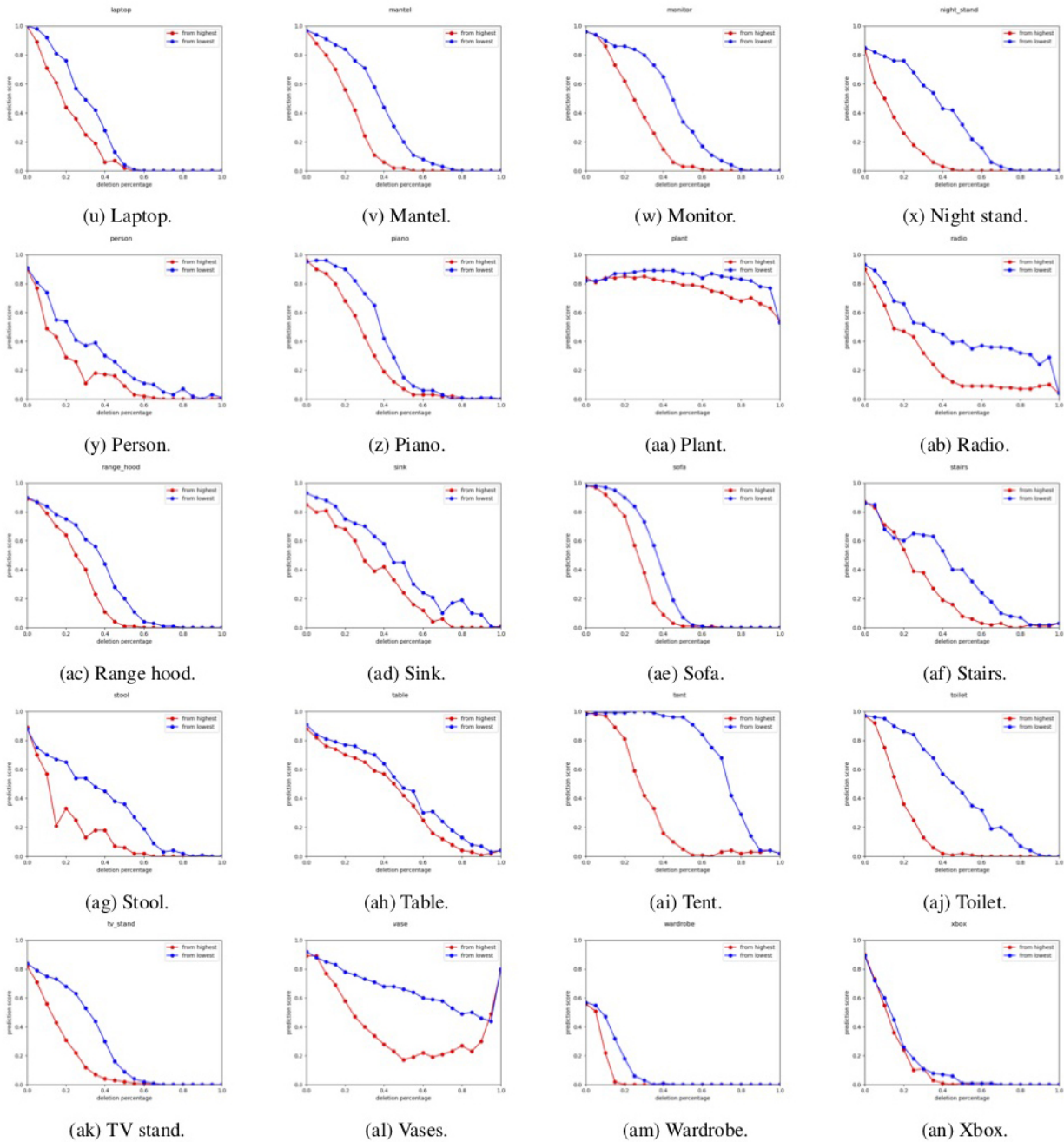


Figure 9: *Deletion* and *insertion* curves for all 40 classes in ModelNet40 for PointConv. Horizontal axis is the deletion percentage (top 5%, 10%, etc.), and vertical axis is the predicted class score. The red line is the *deletion* curve which blurs points from highest mask values, and the blue line is the *insertion* curve (if read from right to left) which blurs points from lowest mask values. (cont.)



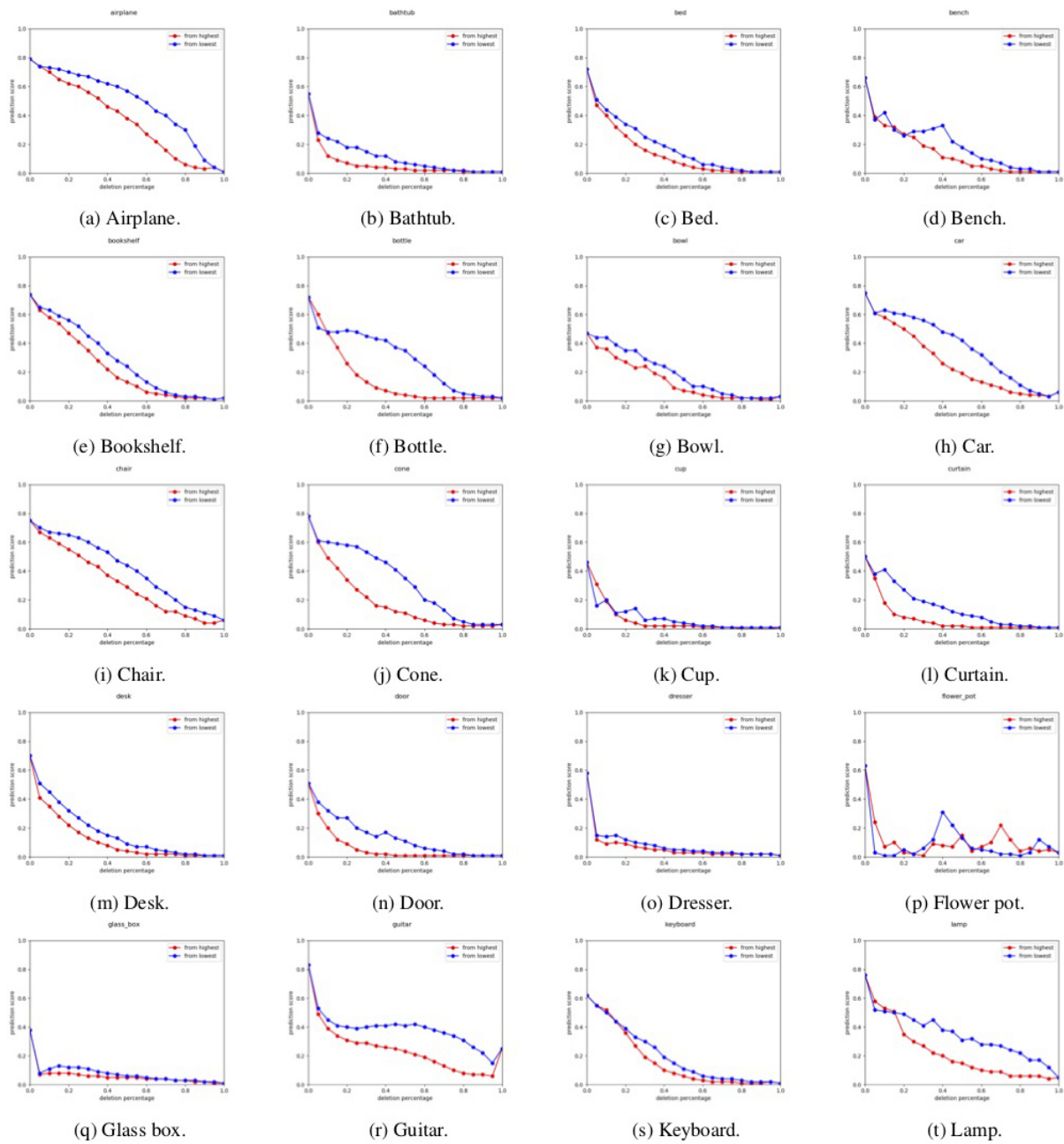


Figure 10: *Deletion* and *insertion* curves for all 40 classes in ModelNet40 for DGCNN. Horizontal axis is the deletion percentage (top 5%, 10%, etc.), and vertical axis is the predicted class score. The red line is the *deletion* curve which blurs points from highest mask values, and the blue line is the *insertion* curve (if read from right to left) which blurs points from lowest mask values.

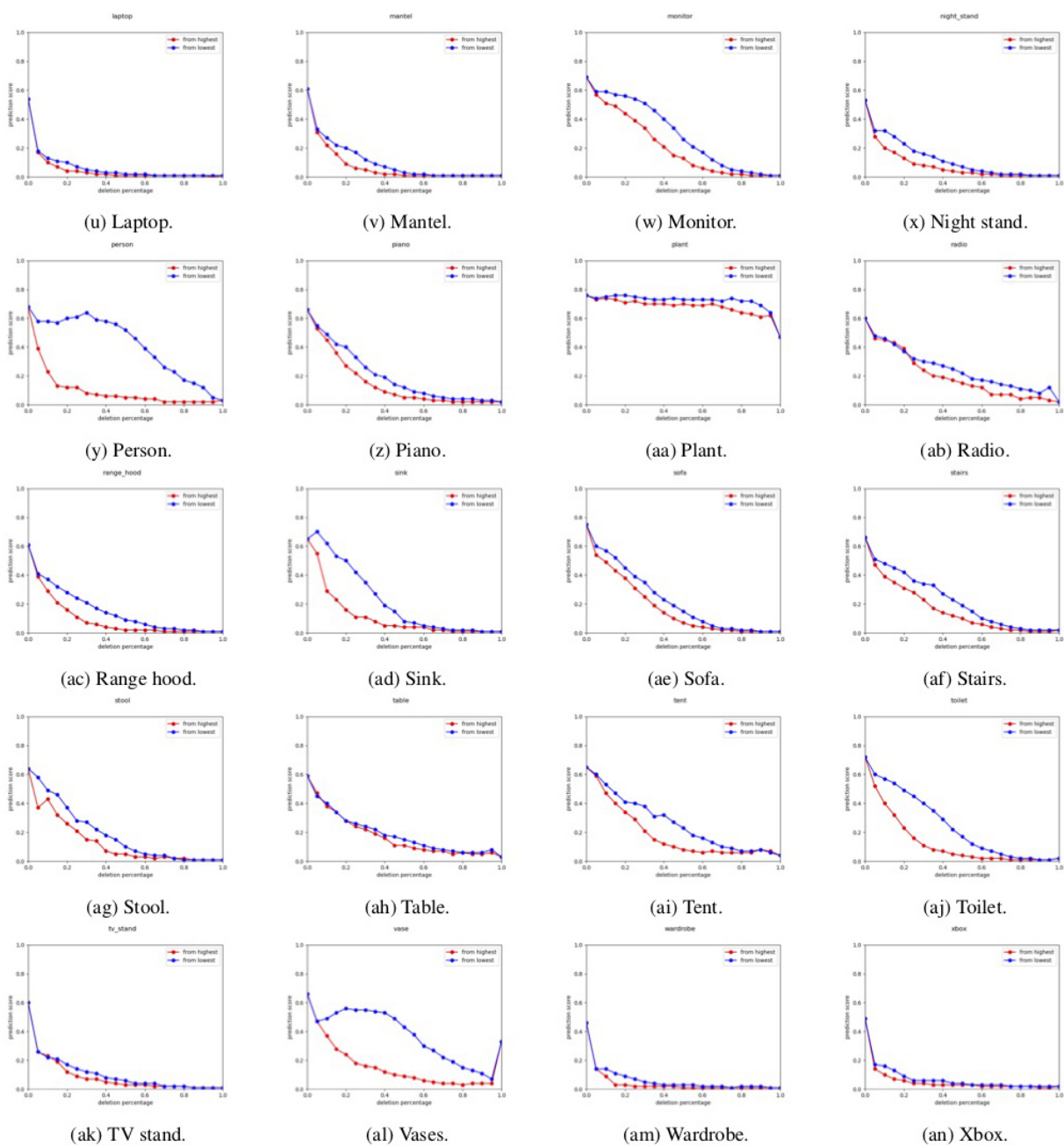


Figure 10: *Deletion* and *insertion* curves for all 40 classes in ModelNet40 for DGCNN. Horizontal axis is the deletion percentage (top 5%, 10%, etc.), and vertical axis is the predicted class score. The red line is the *deletion* curve which blurs points from highest mask values, and the blue line is the *insertion* curve (if read from right to left) which blurs points from lowest mask values. (cont.)